

# PCCP

Accepted Manuscript



This is an *Accepted Manuscript*, which has been through the Royal Society of Chemistry peer review process and has been accepted for publication.

*Accepted Manuscripts* are published online shortly after acceptance, before technical editing, formatting and proof reading. Using this free service, authors can make their results available to the community, in citable form, before we publish the edited article. We will replace this *Accepted Manuscript* with the edited and formatted *Advance Article* as soon as it is available.

You can find more information about *Accepted Manuscripts* in the [Information for Authors](#).

Please note that technical editing may introduce minor changes to the text and/or graphics, which may alter content. The journal's standard [Terms & Conditions](#) and the [Ethical guidelines](#) still apply. In no event shall the Royal Society of Chemistry be held responsible for any errors or omissions in this *Accepted Manuscript* or any consequences arising from the use of any information it contains.

# DFT+U studies of Cu doping and p-type compensation in crystalline and amorphous ZnS

Hieu H. Pham<sup>a</sup>, Gerard T. Barkema<sup>b</sup>, Lin-Wang Wang<sup>a\*</sup>

<sup>a</sup> Joint Center for Artificial Photosynthesis and Materials Sciences Division

Lawrence Berkeley National Laboratory, Berkeley, California 94720, USA

<sup>b</sup> Theoretical Physics, Utrecht University, Leuvenlaan 4, 3584 CE Utrecht, The Netherlands

## Abstract

Zinc sulfide is an excellent candidate for the development of a p-type transparent conducting material that has great demands in solar energy and optoelectronic applications. Doping with Cu is one potential way to make ZnS p-type while preserving its optical transparency for solar spectrum; however, this is limited by the extremely low solubility of Cu in ZnS and charge compensation mechanisms that eliminate the p-type-ness. These mechanisms are various in crystalline (c-ZnS) and amorphous structures (a-ZnS), leading to different tendencies of doping Cu in these two ZnS phases, as well as the feasibility to form the p-type material. In this work, we have carried out fundamental studies of Cu doping in both c-ZnS and a-ZnS, using the continuous random network model and density functional theory with Hubbard's energy correction (DFT+U). The formation of a complex that contains two Cu<sub>Zn</sub> and one S vacancy is highly favorable in both phases. The local environment of this charge-compensated Cu complex obtained by DFT calculations agrees well with previous EXAFS measurements. The incorporation of Cu into a-ZnS, on the one hand, is more tolerable compared to their crystal counterparts (zincblende), indicating possible higher Cu concentration. On the other hand, there is also another intrinsic mechanism to compensate the p-type-ness in a-ZnS: the formation of the covalent S-S "dumbbell" units. This reconstruction of local structure to form the S-S bond could happen spontaneously, thus make the p-type doping for ZnS challenging even in the amorphous phase.

**Keywords:** hole conduction, transparent conducting materials, optical properties, electronic structure, solar cells, charge compensation

\*Corresponding Author: Lin-Wang Wang (lwwang@lbl.gov)

## 1. Introduction

Transparent conducting materials (TCMs) play an essential role in the performance of many devices for electronic applications, including photovoltaics, light emitting diodes and transparent thin film transistors [1, 2]. However, only n-type TCMs have been successfully developed to date for commercial use; for example, impurity-doped zinc oxide, indium oxide and tin oxide are among the most popular ones [3]. The development of p-type TCM thin films, including oxides with delafossite structure (e.g.  $\text{CuMO}_2$ ,  $\text{AgMO}_2$ ,  $M = \text{trivalent cation}$ ), spinel structure (e.g.  $\text{NiCo}_2\text{O}_4$ ), mixed oxides, (e.g.  $\text{In}_2\text{O}_3\text{-Ag}_2\text{O}$ ,  $\text{SnO}_2$ ) and non-oxide materials (e.g.  $\text{BaCu}_2\text{S}_2$ ) etc. [2, 4-6], is still an active research area since the first report of high p-type conductivity in  $\text{CuAlO}_2$  [7]. In fact, developing p-type TCMs is difficult because many transparent materials have relatively low valence band edge, which make it difficult to be doped as p-type due to either the doping limit rules [8, 9] or compensation mechanisms [10]. But for many junction device applications, both n-type and p-type TCMs are essential [7, 11, 12]. ZnS-based materials have been extensively studied and have shown their promises for this purpose [13-16]. They have a suitable band gap that guarantees no absorption in the visible range, however exhibit a limited conductivity. Copper sulfide materials  $\text{Cu}_x\text{S}$ , on the contrary, are highly conductive but not transparent to wavelengths in the solar spectrum, due to their small band gap [17]. Many attempts have been made to dope Cu into the ZnS matrix to improve the conductivity [12, 18]. The challenge here partially lies in the significant dissimilarity in the crystal structures of zinc sulfide and copper sulfide that makes their alloys difficult to attain. As a result, Cu is only soluble in ZnS up to a concentration of about 400 ppm [19]. Instead, Cu would be found either near the surface of the ZnS nanoparticles or in phase separated CuS or  $\text{Cu}_2\text{S}$  precipitates [19-21]. One common technique is to use co-activators such as  $\text{Al}^{3+}$ ,  $\text{Ga}^{3+}$ ,  $\text{In}^{3+}$ ,  $\text{Cl}^-$  or  $\text{Br}^-$  for charge compensation to stabilize Cu in the host lattice [22]. Besides the difficulty to dope the ZnS with Cu, another problem is the formation of compensating defects (or defect complexes), which can kill the charge carriers (holes). Another issue that has drawn some attention is the formation of highly disordered phases, i.e. amorphous structures. The dopability in crystalline and amorphous structures could be drastically different, so are their typical charge compensation mechanisms. In general, the introduction of holes depends on multiple factors; including the formation and ionization energy of charge producing defects, as well as the formation energy of charge killing defects [23]. Therefore, it would be interesting to know

whether it is more favorable or challenging to form p-type ZnS in amorphous structure, in regard to both Cu doping limits and charge balance mechanisms. In this work, we will investigate the structural characterizations, electronic properties and several typical p-type compensation models of Cu doping in both crystalline (zincblende c-ZnS) and amorphous (a-ZnS) phases, with first principles calculations.

Relative to the crystalline counterparts, the amorphous structures are highly favorable for solar cells and flat-panel display applications, due to the cost-effectiveness of growth and deposition techniques as well as their ability to form a smooth interface with large-area substrates of different lattice constants [24]. In fact, the low-temperature synthesis of amorphous materials has become standard and their use is ubiquitous. It was shown that the amorphous films could exhibit superior properties and significantly improve the performance of many photoelectric devices [24-27]. Additionally, experimental studies have suggested that the nanoparticles or quantum dots, which have been extensively investigated for next-generation solid-state lighting applications, favorably adopt the core-shell structure, and the shell is often composed of the amorphous phase [27-30]. While the tendency of forming p-type c-ZnS and compensation mechanisms that eliminate the p-type-ness have been investigated both experimentally and theoretically [12, 31], the situation in a-ZnS is rather unknown.

The study of the amorphous materials is nontrivial because the definition of a realistic amorphous structure could be ambiguous. Here we have employed a continuous random network approach (CRN) to construct well-relaxed atomic configurations of a model amorphous ZnS. The electronic structure of this Cu-doped ZnS system, together with its zincblende counterpart, is then investigated by density functional theory (DFT), including the hybrid functional (HSE06) [32] and the GGA+U [33]. The Cu doping and alloying in wurtzite ZnS have also been studied by our group through *ab initio* calculations [12]. It was found that the most predominant defect is  $\text{Cu}_{\text{Zn}}$  antisite when the Fermi energy is above the valence band edge. However, this previous study has not address the issue of amorphous structure and charge-compensated complexes such as  $\text{V}_{\text{S}}\text{Cu}_{\text{Zn}}\text{Cu}_{\text{Zn}}$ . Those are the issues we investigate in this work and we find that: i) Despite the structural disorder, the CRN amorphous ZnS model has no mid-gap states (even though its band gap is narrower than its crystal counterpart); ii) The formation energy of Cu dopant in the amorphous ZnS is significantly lower than that in the zincblende system, which suggests a higher solubility of Cu in the amorphous phase; iii) In both c-ZnS and a-ZnS, the formation of the S

vacancy ( $V_S$ ) adjacent to the  $Cu_{Zn}$  is thermodynamically favorable (by several eV), compared to the separated configurations. In this context, the Cu-S and Zn-S bond distances are reduced as Cu and Zn are pushed away from the S vacancy and towards three remaining S nearest neighbors. This agrees with experimental observation using the EXAFS technique [31]; iv) In the amorphous structure, a hole killer upon Cu doping could be prominent: the formation of covalent S-S “dumbbell” units, which are similar to those in covellite CuS and pyrite-type  $Cu_2S$  structures [34, 35].

## 2. Computational Details

Currently the best approach for the generation of well-relaxed covalent amorphous semiconductors and glasses is the CRN approach of Wooten, Winer and Weaire [36]. Starting from the crystalline diamond structure, local bond switches rapidly transform it into a low-strain amorphous structure free of coordination defects. In this work, the CRN approach, adapted to generate binary alloys [37], was used to generate a number of initial a-ZnS structures containing between 64 and 200 atoms. The obtained systems (amorphous) were then used for further atomic relaxation by first-principles calculations.

Density functional theory (DFT), [38] as implemented in the Vienna *ab initio* Simulation Package (VASP), [39] was employed to perform first-principles calculations. Most calculations used the electron projector-augmented wave methods [40] with the PBE generalized gradient approximation (GGA) exchange-correlation [41], plus on-site Zn and Cu d state U corrections (DFT+U, or say GGA+U) [33], otherwise noted. A plane-wave cut-off of 450 eV was used and the magnetic moment was accounted for by performing spin-polarized energy calculations. The values of  $U = 7.0$  and  $6.0$  were used for the Coulomb corrections to the Zn and Cu 3d states, respectively, that have shown to reproduce well the electronic structure and ground-state properties of ZnS and  $Cu_2O$  [42-44]. For the k-space sampling, we used a  $3 \times 3 \times 3$  Monkhorst-Pack grid [45] for the 64-atom supercells (both c-ZnS and a-ZnS). For hybrid calculations (HSE06), a  $2 \times 2 \times 2$  grid was used.

The formation energy of Cu substitution (Cu replacing Zn) with charge state  $q$  is calculated as follows [46]:

$$\Delta H(Cu^q) = E(Cu^q) - E(clean) - (E_{Cu} + \Delta\mu_{Cu}) + (E_{Zn} + \Delta\mu_{Zn}) + q(\epsilon_{VBM} + E_F + \Delta v) \quad (1)$$

where  $E(Cu^q)$  and  $E(clean)$  are the total energies of the supercells with and without the defect (Cu substitution).  $\Delta\mu_{Cu}$  and  $\Delta\mu_{Zn}$  are the elemental chemical potentials of Cu and Zn, referenced to the DFT elemental energy  $E_{Cu}$  and  $E_{Zn}$  of their ground states (we used the crystal structures of face-centered cubic Cu and hexagonal-closed pack Zn). For simplicity and the purpose of comparison between the crystalline and amorphous models, we assume the metals in their rich conditions, i.e.  $\Delta\mu = 0$  for both Cu and Zn (the formation energy difference between c-ZnS and a-ZnS will not depend on these  $\Delta\mu$ 's).  $E_F$  is the Fermi energy level referenced to the valence band maximum (VBM) eigenenergy of the bulk ZnS system, and  $\epsilon_{VBM}$  is the VBM eigen energy of the bulk system when the averaged Hartree potential is set to zero. The term  $\Delta v$  is added for the correction of the electrostatic potential caused by the limited size of the supercell, obtained from the shifting of the 1s core-level energy of a Zn atom (located far away from the defect site) between the neutral impurity and charged cases. Similar procedure was adopted for the calculation of S vacancy, in which the sulfur-6 structure was used as the ground state  $E_S$ . The values are presented for S poor condition, i.e.  $\Delta\mu_S = \Delta H_f(ZnS) = -2.0$  eV [12] to maintain the thermodynamic equilibrium between Zn, S and ZnS ( $\Delta\mu_{Zn} + \Delta\mu_S = \Delta H_f(ZnS)$ )

### 3. Results and Discussions

#### 3.1. Structural characterization and effects of amorphousness on the band structure

The radial distribution functions (RDF) for Zn-S, Zn-Zn and S-S pairs of the amorphous and zincblende crystals are presented in Figure 1. In fact, CRN amorphous systems of different sizes (containing between 64 and 200 atoms) were also calculated and they have similar structural characteristics after the relaxation by DFT. The first peaks are located at same distances in both phases, which indicates that most of the local Zn-S bonding and tetrahedral ZnS<sub>4</sub> configurations are preserved in the amorphous structure. The distribution of the coordination number for Zn is shown in Figure 2, using a cut-off distance of 2.6 Å. It showed a significant amount of Zn (and S) in a-ZnS that has “non-perfect” coordination number (3-fold instead of 4-fold coordinated). This however slightly depends on the cut-off distance used for defining the bonding.

The calculations on electronic properties of amorphous ZnS to this end will be performed on the 64-atom sample, and for comparison we used a zincblende supercell with the same number of atoms. Interestingly, the amorphous ZnS has a clean band gap (Figure 3) despite a noticeable structural disorder and non-perfect coordination numbers. This is in contrast with

many other covalent-bonded semiconductors, where non-perfect coordination often leads to mid-gap states [47, 48]. In addition, Zn and S contribute to both VBM and CBM in either structure (amorphous and crystalline). In order to correct the well-known band gap underestimation by GGA, we performed additional calculations with the non-local hybrid functional (HSE06) [32], using the pre-optimized structures from the DFT+U method. The hybrid calculation yielded a band gap of 3.45 eV for zincblende ZnS, which is close to the experimental measurements ( $\sim 3.5$  eV) [49, 50]. However, a large reduction of the band gap was observed upon the amorphization (2.75 eV from the HSE06 calculation). The a-ZnS density obtained by DFT+U ( $3.75 \text{ g/cm}^3$ ) is significantly lower than the corresponding zincblende ZnS value of  $4.16 \text{ g/cm}^3$  (the experimental value is  $4.09 \text{ g/cm}^3$  [51]). Despite this difference in density, the average Zn-S bond distance in the amorphous phase ( $d^{\text{avg}} = 2.35 \text{ \AA}$ , calculated for all 4-fold coordinated Zn) is still comparable to that in the crystal ( $2.32 \text{ \AA}$ ). Further experimental verification is probably needed to shed light on whether the band gap reduction is caused by the “imperfectness” of the amorphous model, or is an intrinsic feature of the ZnS amorphous structure.

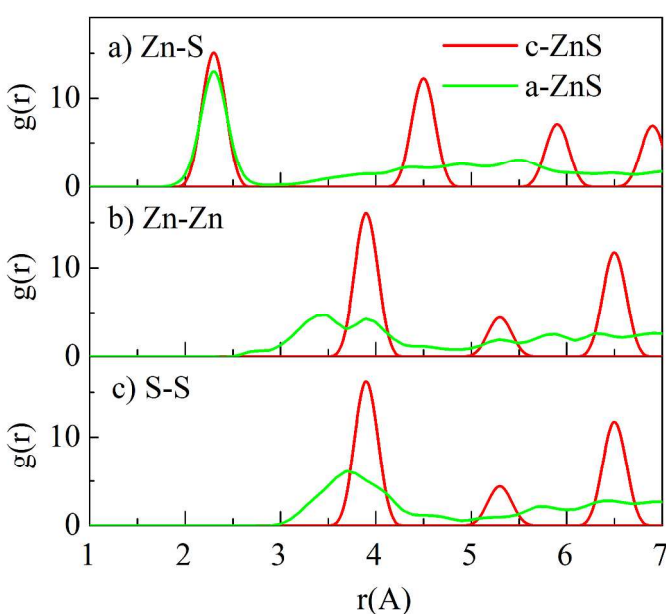


Figure 1. Radial distribution functions  $g(r)$  for a) Zn-S, b) Zn-Zn and c) S-S pairs of the zincblende (c-ZnS) and amorphous (a-ZnS) zinc sulfide models

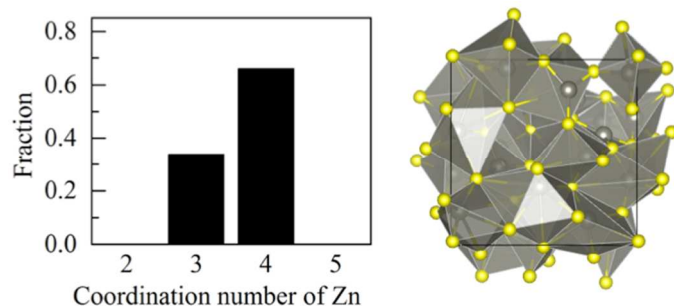


Figure 2. Coordination number distribution of Zn (left) and the relaxed structure of the 64-atom amorphous ZnS model (right). The cutoff distance for calculating the neighbors  $r = 2.6 \text{ \AA}$  and DFT+U was used for the atomic relaxation after the structure was generated by CRN method. Dark sphere – Zn, light sphere – S

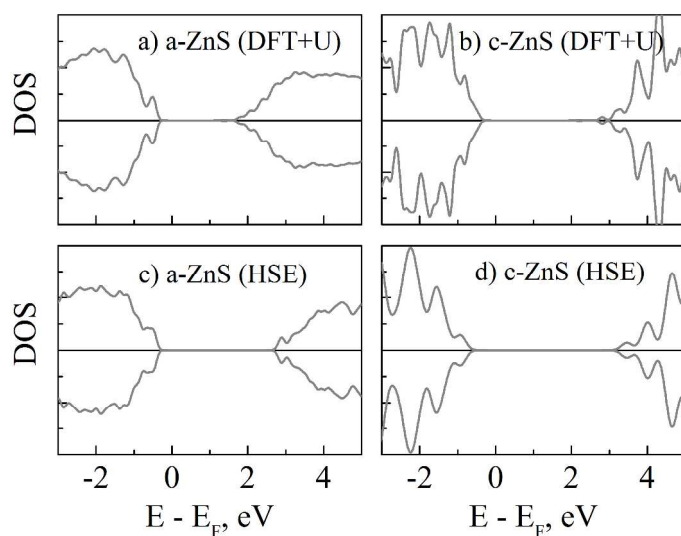


Figure 3. Density of states of crystalline and amorphous ZnS calculated using DFT+U and HSE06. The pre-optimized structures obtained from DFT+U were used for the hybrid calculations

### 3.2. Cu doping in crystalline and amorphous ZnS

Figure 4 displays the formation energy calculations for  $\text{Cu}_{\text{Zn}}$  (substitution of Zn by Cu) and  $\text{V}_{\text{S}}$  (S vacancy) defects in the amorphous and zincblende ZnS at various charge states. Note that, in a-ZnS case there are different sites to replace Zn and or remove S, that could yield different formation energies. The reported values in Figure 4 are the lowest formation energy ones for the corresponding impurity species. They represent possible defect sites in an actual amorphous

system. The defect sites were chosen as described in the following. It was seen that the valence band maximum (VBM) and conduction band minimum (CBM) states of the amorphous ZnS are localized on some sulfur and zinc atoms respectively, instead of being delocalized all over the supercell. Those Zn and S are then used as the most favorable sites for the corresponding defect formation. Our calculations indicated that they all follow the trend in which the formation of defects in a-ZnS is energetically more favorable than their crystalline counterparts. This observation is consistent with what reported for other amorphous materials [52]. This further suggests that Cu solubility limit could be higher in the amorphous phase. Also, the acceptor ionization level (transition energy levels from  $\text{Cu}_{\text{Zn}}^0$  to  $\text{Cu}_{\text{Zn}}^{1-}$ , Figure 4) is slightly shallower in a-ZnS, compared to that in c-ZnS.

Our calculations show that the substitution of Zn by Cu results in a hole in valence band, indicating the presence of  $\text{Cu}^{1+}$  (in other notation,  $\text{Cu}_{\text{Zn}}^{1-}$ ) instead of  $\text{Cu}^{2+}$ . The Fermi level is shifted into the valence band in which the shifting depth depends on the amount of Cu content (Figure 5a-d). This electronic characterization denotes a p-type metallic conductor [49]. The density of states (DOS) calculations also showed that the incorporation of Cu only makes contributions to the valence band edge that slightly narrow the band gap (in both crystalline and amorphous systems), instead of inducing any mid-gap states.

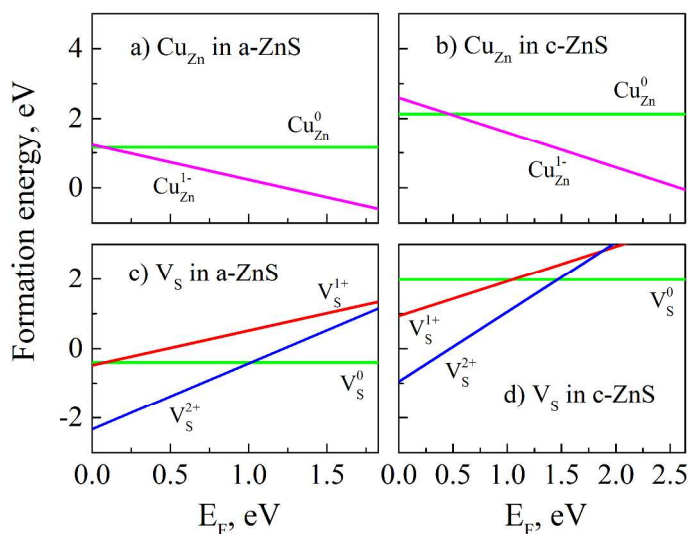


Figure 4. Formation energy of Cu substitution ( $\text{Cu}_{\text{Zn}}$ ) and S vacancy ( $\text{V}_{\text{S}}$ ) as a function of Fermi energy in: (a,c) amorphous ZnS and (b,d) crystalline ZnS. The crossing points show the transition energy levels between different charge states. Positive slope means positively charged

state, while negative slope corresponds to negatively charged state. The results (GGA+U) were calculated for Cu-rich, Zn-rich and S-poor conditions

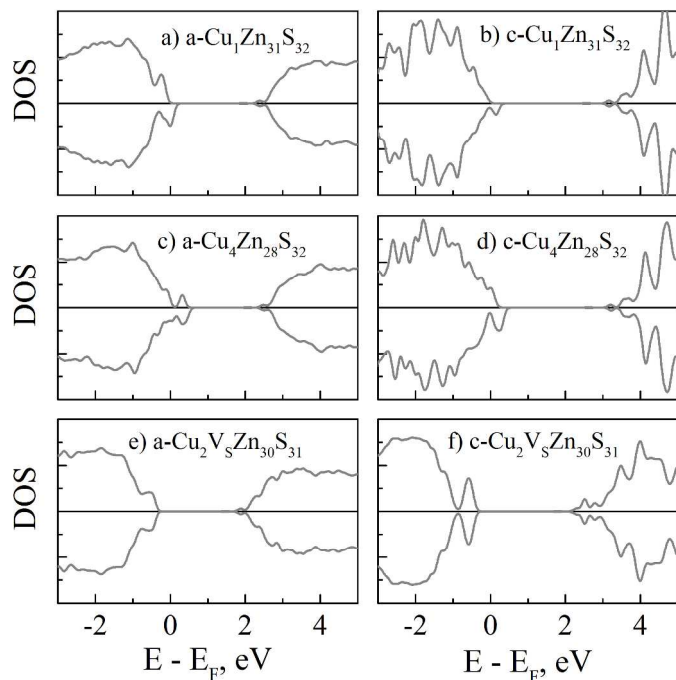


Figure 5. Density of states of amorphous (a-ZnS) and zincblende (c-ZnS) at different Cu contents (DFT+U calculations). In figures (c-d), four Cu atoms substitute Zn at corners of the same Zn-S tetrahedron. In figures (e-f), the complex (of two  $\text{Cu}_{\text{Zn}}$  and the S vacancy) also belongs to same tetrahedron configuration (as shown in Figure 6d)

### 3.3. Intrinsic charge compensation models for Cu doping: S vacancy and S-S bonding

**Charge-compensated complex of an S vacancy and two substitutional Cu ( $V_{\text{S}}\text{Cu}_{\text{Zn}}\text{Cu}_{\text{Zn}}$ ).** It is believed that the doping of Cu could be significantly enhanced if there were a mechanism to balance the charges (holes) induced by its +1 oxidation state, thus helps stabilize the Cu in host lattice ZnS. Figure 4 presented the calculations of separate  $V_{\text{S}}$  and  $\text{Cu}_{\text{Zn}}$ . When the Fermi energy is close to the valence band edge, the formation of a  $V_{\text{S}}^{2+}$  (which can compensate the free hole carrier) in c-ZnS is not very likely (only has a rather small negative formation energy). Meanwhile, its introduction in a-ZnS is more feasible (with a large negative formation energy). Nevertheless, the possibility of defect clusters was not considered in Figure 4. Based on experimental measurements, many such complexes have been proposed, including: two  $\text{Cu}_{\text{Zn}}^{1-}$

adjacent to a sulfur vacancy  $V_S^{2+}$ , one  $Cu_{Zn}^{1-}$  next to a  $Cl_S^{1+}$  (substitution of S by Cl), and a complex of two  $Cu_{Zn}^{1-}$  and one interstitial  $Cu_i^{2+}$  [31]. Here, we will only investigate the situation of two  $Cu_{Zn}^{1-}$  adjacent to a sulfur vacancy  $V_S^{2+}$ . In Figure 6, we present the local structural relaxation induced by the S vacancy in the zincblende system. When the sulfur atom is removed at its neutral state ( $V_S^0$ ), the surrounding Zn's are relaxed towards the vacancy site, subsequently increasing the bond distance with neighboring S's (Figure 6b). However, under  $V_S^{2+}$ , the neighbor Zn is instead displaced away from the vacancy and could be found near the center of the three remaining S atoms with shortened Zn-S bonds (Figure 6c). The preference of this flat triangle arrangement over the tetrahedral symmetry is likely originated from the transition from  $sp^3$  into the  $sp^2$  electron configuration as two electrons are missing. The local environments are comparable between those in Figure 6c and Figure 6d, where two substitutional Cu are further introduced (which implies the Cu in +1 charge state, or  $Cu_{Zn}^{1-}$ ). The relaxation of the Zn atom to the planar configuration is not caused by the Cu substitutions per se, but by the loss of electrons to the two nearby  $Cu_{Zn}$  defects, thus forming an effective  $V_S^{2+}$  for the Zn-3S motif. As a result, the flat Cu-3S configurations are also formed. Our calculations showed that when this  $V_S Cu_{Zn} Cu_{Zn}$  complex is formed, the defect formation energy is reduced by  $\Delta E_f \approx 3.8$  eV and 1.3 eV respectively, compared to the case of separate neutral and charged  $Cu_{Zn}$  and  $V_S$  defects. This off-center displacement of Cu found by our theoretical calculations is consistent with experimental observations by Car et al. using the extended X-ray absorption fine structure measurements (EXAFS) of Cu doping in ZnS nanocrystals [31]. We also observed the tendency of this  $V_S Cu_{Zn} Cu_{Zn}$  complex formation in amorphous ZnS. However, lower  $\Delta E_f$  values ( $\sim 2.0$  eV and 40 meV respectively, compared to the case of separate neutral and charged defects) indicate that this mechanism of hole compensation could be less pronounced in the amorphous structure.

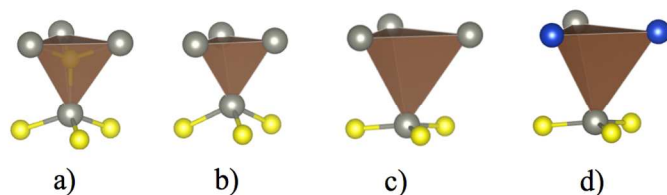


Figure 6. Local structural relaxation induced by the S vacancy ( $V_S$ ) in crystalline ZnS: a) the perfect zinc blende structure, b) the S vacancy at neutral charge state  $V_S^0$ , c) the S vacancy at its ionic state  $V_S^{2+}$ , d) the S vacancy in the complex with two neighboring  $Cu_{Zn}$ . In c) and d), both

Zn and Cu are displaced away from the S vacancy and form planar configurations with three remaining S. Gray sphere – Zn, blue – Cu, yellow – S

**Covalent S-S “dumbbell” pairs.** In this subsection, we will discuss another prominent mechanism for charge balance that was seen in our a-ZnS simulations. The structure optimization of the amorphous phase with high Cu doping has suggested the possibility for the presence of S-S pairs (Figure 7c), which normally exist in crystals such as covellite CuS and pyrite-type Cu<sub>2</sub>S [34, 35]. If this S-S bond is covalent, each of these “dumbbell” units can expectedly balance the charges induced by two Cu<sub>Zn</sub><sup>1-</sup> (that correspondingly produce two valence band holes). Figure 7 displayed the DOS of the amorphous supercell that contains two Cu<sub>Zn</sub>, before and after the formation of S-S bond. The S-S bond distance (Figure 7c) was measured at approximately 2.1 Å, comparable to that in both covellite and pyrite copper sulfide [34, 35]. It showed that the original hole states disappear after the S-S bond is formed. Upon the formation of the S-S dumbbell pair, two empty states start rising into the middle of the band gap and finally merge into the conduction band (Figure 7b-c). The formation energy of this S-S bond in the amorphous structure is  $E_f^{S-S} = -1.45 \text{ eV}$ . Due to this negative value, the formation of the Cu<sub>Zn</sub>Cu<sub>Zn</sub>(S-S) complex in a-ZnS could be automatic as its energy ( $E_f^{comp} = 1.89 \text{ eV}$ ) is smaller than that of two substitutional Cu<sub>Zn</sub> without the S-S bonding pair ( $E_f^{2Cu} = 2.33 \text{ eV}$ ). These values in c-ZnS are  $E_f^{S-S} = 1.20 \text{ eV}$  and  $E_f^{comp} = 5.35 \text{ eV}$ , respectively. These numbers indicate that the formation of S-S dumbbell units could be more pronounced in a-ZnS and not likely in c-ZnS. Note that, the introduction of S-S bonding pair should be intrinsically easier compared to the V<sub>S</sub> formation, since it only involves the local distortion of surrounding atoms and does not require long distance migration of S (to yield the vacancy). Our calculations using the nudged elastic band method [53] suggested that, the structure relaxation (around Cu<sub>Zn</sub>) to form the S-S covalent bond in a-ZnS could happen spontaneously without any energy barrier in some cases.

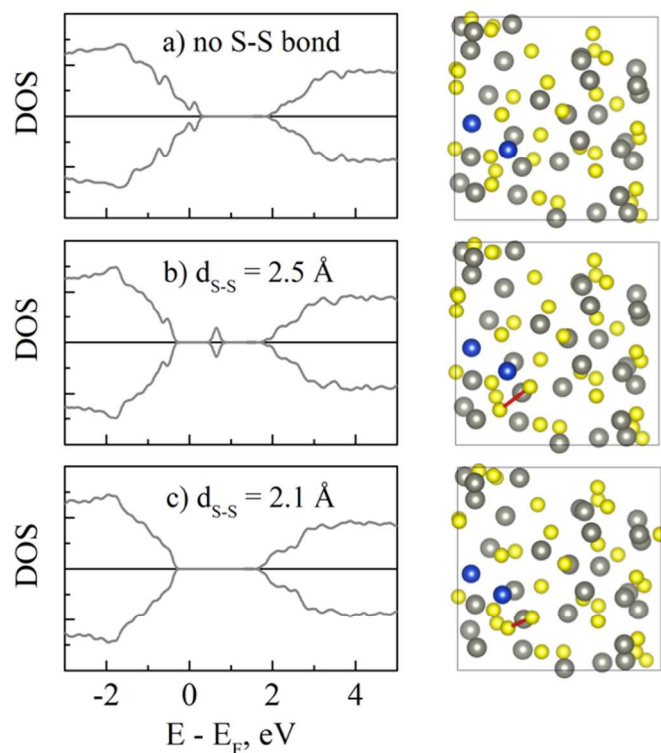


Figure 7. The disappearance of hole states (at the VBM) by the formation of S-S bond in the amorphous structure ( $\text{Cu}_2\text{Zn}_{30}\text{S}_{32}$ ). Two holes exist when two substitutional Cu's are introduced (a), but as a S-S pair distance reduces (the red line, from (b) to (c)), those hole states rise up and disappear into the conduction band (c). Gray sphere – Zn, blue – Cu, yellow – S.

#### 4. Conclusions

In summary, we have investigated the Cu doping in both crystalline and amorphous zinc sulfide by the continuous random network model and density functional theory calculations. In the amorphous ZnS structure, the nearest neighbor Zn-S bonding and local tetrahedral configurations are preserved. The long-range disorder and imperfect coordination of Zn and S do not induce defect states but do reduce the band gap, and also results in the wave function localization of the band edge states. The cost of doping in a-ZnS is energetically more favorable (easier) compared to c-ZnS, probably due to the intrinsic structural disorder and bonding frustration. Each substitution of Zn by Cu introduces a valence band hole, which indicates the +1 oxidation state of Cu and expectedly makes the material a metallic conductor of p-type.

However, there are various mechanisms that could readily compensate these hole states in both crystalline and amorphous ZnS, thus reduce the likelihood of p-type doping. One is the

presence of sulfur vacancy at 2+ charge state ( $V_S^{2+}$ ) when the Fermi energy is close to the valence band edge (p-type). This is particularly true for a-ZnS. Besides, the formation of the  $V_S^{2+}Cu_{Zn}^{1-}Cu_{Zn}^{1-}$  complex, which has much lower formation energy than that of separated defects, could be more prominent in eliminating the hole carriers. In this defect complex, neighboring Cu and Zn are displaced away from the vacancy and towards the remaining S, forming a planar  $sp^2$  configuration, which is consistent with experimental EXAFS observations [31]. In addition, another hole killing mechanism is the formation of the covalent S-S bonds in a-ZnS. When the Fermi energy is near the valence band edge, we found that the formation energy of the S-S pair is negative in a-ZnS, and the spontaneous formation of this S-S dumbbell without a kinetic barrier height could be possible. While the former mechanism ( $V_S$  defect and  $V_S$  complex in c-ZnS) was already proposed by experiments [31], the latter one (S-S pair) in a-ZnS needs further experimental investigations. All in all, we find that, while it is energetically easier to dope a-ZnS with Cu compared to c-ZnS, there are also more mechanisms to compensate the p-type hole carriers in a-ZnS.

#### ACKNOWLEDGMENTS

We would like to thank Dr. Shiyu Chen, Dr. Jason Cooper, Dr. Joel Ager, Dr. Jie Ma, Dr. Danylo Zherebetsky, Rachel Woods-Robinson and Xiaojie Xu for helpful discussions. This material is based on the work performed by the Joint Center for Artificial Photosynthesis, a DOE Energy Innovation Hub, supported through the Office of Science of the U.S. Department of Energy under Award number DE-SC0004993. We use the resource of National Energy Research Scientific Computing center (NERSC) located in Lawrence Berkeley National Laboratory.

## REFERENCES

1. Hosono, H., *Recent progress in transparent oxide semiconductors: Materials and device application*. Thin Solid Films, 2007. **515**(15): p. 6000-6014.
2. Banerjee, A.N. and K.K. Chattopadhyay, *Recent developments in the emerging field of crystalline p-type transparent conducting oxide thin films*. Progress in Crystal Growth and Characterization of Materials, 2005. **50**(1-3): p. 52-105.
3. Minami, T., *Transparent conducting oxide semiconductors for transparent electrodes*. Semiconductor Science and Technology, 2005. **20**(4): p. S35-S44.
4. Scanlon, D.O., A. Walsh, and G.W. Watson, *Understanding the p-Type Conduction Properties of the Transparent Conducting Oxide CuBO<sub>2</sub>: A Density Functional Theory Analysis*. Chemistry of Materials, 2009. **21**(19): p. 4568-4576.
5. Yang, T.Y., et al., *Preparation and application in p-n homojunction diode of p-type transparent conducting Ga-doped SnO<sub>2</sub> thin films*. Thin Solid Films, 2010. **518**(19): p. 5542-5545.
6. Banerjee, A.N., S.W. Joo, and B.K. Min, *Quantum size effect in the photoluminescence properties of p-type semiconducting transparent CuAlO<sub>2</sub> nanoparticles*. Journal of Applied Physics, 2012. **112**(11).
7. Kawazoe, H., et al., *P-type electrical conduction in transparent thin films of CuAlO<sub>2</sub>*. Nature, 1997. **389**(6654): p. 939-942.
8. Zunger, A., *Practical doping principles*. Applied Physics Letters, 2003. **83**(1): p. 57-59.
9. Lany, S. and A. Zunger, *Dopability, intrinsic conductivity, and nonstoichiometry of transparent conducting oxides*. Physical Review Letters, 2007. **98**(4).
10. Zhang, S.B., S.H. Wei, and A. Zunger, *Intrinsic n-type versus p-type doping asymmetry and the defect physics of ZnO*. Physical Review B, 2001. **63**(7).
11. Sato, H., et al., *Transparent Conducting P-Type NiO Thin-Films Prepared by Magnetron Sputtering*. Thin Solid Films, 1993. **236**(1-2): p. 27-31.
12. Diamond, A.M., et al., *Copper-alloyed ZnS as a p-type transparent conducting material*. Physica Status Solidi a-Applications and Materials Science, 2012. **209**(11): p. 2101-2107.
13. Akhtar, M.S., et al., *Structural, optical, magnetic and half-metallic studies of cobalt doped ZnS thin films deposited via chemical bath deposition (vol 3, pg 6755, 2015)*. Journal of Materials Chemistry C, 2015. **3**(27): p. 7228-7228.
14. Akhtar, M.S., et al., *Chemical bath deposition of Fe-doped ZnS thin films: Investigations of their ferromagnetic and half-metallic properties*. Materials Science in Semiconductor Processing, 2015. **39**: p. 283-291.
15. Akhtar, M.S., et al., *Room temperature ferromagnetism and half metallicity in nickel doped ZnS: Experimental and DFT studies*. Materials Chemistry and Physics, 2015. **160**: p. 440-446.
16. Revaprasadu, N., et al., *Deposition of zinc sulfide quantum dots from a single-source molecular precursor*. Journal of Materials Research, 1999. **14**(8): p. 3237-3240.
17. Klimov, V., et al., *Linear and Nonlinear Transmission of Cuxs Quantum Dots*. Applied Physics Letters, 1995. **67**(5): p. 653-655.
18. Woods-Robinson, R., et al. *Carrier scattering mechanisms in p-type transparent copper-alloyed ZnS: Crystalline vs. amorphous*. in *APS Meeting Abstracts*. 2015.
19. Stanley, J., et al., *Degradation and rejuvenation studies of AC electroluminescent ZnS:Cu,Cl phosphors*. Journal of Physics-Condensed Matter, 2010. **22**(5).

20. Corrado, C., et al., *Synthesis and Characterization of Organically Soluble Cu-Doped ZnS Nanocrystals with Br Co-activator*. Journal of Physical Chemistry C, 2011. **115**(30): p. 14559-14570.
21. Corrado, C., et al., *Synthesis, Structural, and Optical Properties of Stable ZnS:Cu,Cl Nanocrystals*. Journal of Physical Chemistry A, 2009. **113**(16): p. 3830-3839.
22. Gul, S., et al., *Effect of Al<sup>3+</sup> Co-doping on the Dopant Local Structure, Optical Properties, and Exciton Dynamics in Cu<sup>+</sup>-Doped ZnSe Nanocrystals*. ACS Nano, 2013. **7**(10): p. 8680-8692.
23. Raebiger, H., S. Lany, and A. Zunger, *Origins of the p-type nature and cation deficiency in Cu<sub>2</sub>O and related materials*. Physical Review B, 2007. **76**(4).
24. Narushima, S., et al., *A p-type amorphous oxide semiconductor and room temperature fabrication of amorphous oxide p-n heterojunction diodes*. Advanced Materials, 2003. **15**(17): p. 1409-1413.
25. Pham, H.H. and L.W. Wang, *Oxygen vacancy and hole conduction in amorphous TiO<sub>2</sub>*. Physical Chemistry Chemical Physics, 2015. **17**(1): p. 541-550.
26. Walsh, A., J.L.F. Da Silva, and S.H. Wei, *Interplay between Order and Disorder in the High Performance of Amorphous Transparent Conducting Oxides*. Chemistry of Materials, 2009. **21**(21): p. 5119-5124.
27. Sun, L.D. and Q. Wang, *PbS Quantum Dots Capped with Amorphous ZnS for Bulk Heterojunction Solar Cells: The Solvent Effect*. ACS Applied Materials & Interfaces, 2014. **6**(16): p. 14239-14246.
28. Barnard, A.S., C.A. Feigl, and S.P. Russo, *Morphological and phase stability of zinc blende, amorphous and mixed core-shell ZnS nanoparticles*. Nanoscale, 2010. **2**(10): p. 2294-2301.
29. Zhang, H.Z., et al., *Water-driven structure transformation in nanoparticles at room temperature*. Nature, 2003. **424**(6952): p. 1025-1029.
30. Jason K. Cooper, S.G., Sarah A. Lindley, Junko Yano, and Jin Z. Zhang, *Tunable Photoluminescent Core/Shell Cu<sup>+</sup>-Doped ZnSe/ZnS Quantum Dots Codoped with Al<sup>3+</sup>, Ga<sup>3+</sup>, or In<sup>3+</sup>*. ACS Applied Materials & Interfaces, 2015. **7**(18): p. 10055-10066.
31. Car, B., et al., *Probing the local structure of dilute Cu dopants in fluorescent ZnS nanocrystals using EXAFS*. Nanoscale, 2011. **3**(10): p. 4182-4189.
32. Paier, J., et al., *Screened hybrid density functionals applied to solids (vol 124, pg 154709 2006)*. Journal of Chemical Physics, 2006. **125**(24): p. 249901.
33. Dudarev, S.L., et al., *Electron-energy-loss spectra and the structural stability of nickel oxide: An LSDA+U study*. Physical Review B, 1998. **57**(3): p. 1505-1509.
34. Gotsis, H.J., A.C. Barnes, and P. Strange, *Experimental and Theoretical Investigation of the Crystal-Structure of Cus*. Journal of Physics-Condensed Matter, 1992. **4**(50): p. 10461-10468.
35. Vanderlaan, G., et al., *Oxidation-State Variations in Copper Minerals Studied with Cu 2p X-Ray Absorption-Spectroscopy*. Journal of Physics and Chemistry of Solids, 1992. **53**(9): p. 1185-1190.
36. Wooten, F., K. Winer, and D. Weaire, *Computer-Generation of Structural Models of Amorphous Si and Ge*. Physical Review Letters, 1985. **54**(13): p. 1392-1395.
37. Mousseau, N. and G.T. Barkema, *Fast bond-transposition algorithms for generating covalent amorphous structures*. Current Opinion in Solid State & Materials Science, 2001. **5**(6): p. 497-502.

38. Kohn, W. and L.J. Sham, *Self-Consistent Equations Including Exchange and Correlation Effects*. Physical Review, 1965. **140**(4A): p. 1133-1138.
39. Kresse, G. and J. Furthmuller, *Efficient iterative schemes for ab initio total-energy calculations using a plane-wave basis set*. Physical Review B, 1996. **54**(16): p. 11169-11186.
40. Blochl, P.E., *Projector Augmented-Wave Method*. Physical Review B, 1994. **50**(24): p. 17953-17979.
41. Perdew, J.P., K. Burke, and M. Ernzerhof, *Generalized gradient approximation made simple*. Physical Review Letters, 1996. **77**(18): p. 3865-3868.
42. Tang, J.P., et al., *First principles study on magnetic properties in ZnS doped with palladium*. European Physical Journal B, 2013. **86**(8).
43. Miyake, T., et al., *Quasiparticle energy of semicore d electrons in ZnS: Combined LDA+U and GW approach*. Physical Review B, 2006. **74**(24).
44. Isseroff, L.Y. and E.A. Carter, *Importance of reference Hamiltonians containing exact exchange for accurate one-shot GW calculations of Cu<sub>2</sub>O*. Physical Review B, 2012. **85**(23).
45. Monkhorst, H.J. and J.D. Pack, *Special Points for Brillouin-Zone Integrations*. Physical Review B, 1976. **13**(12): p. 5188-5192.
46. Lany, S. and A. Zunger, *Polaronic hole localization and multiple hole binding of acceptors in oxide wide-gap semiconductors*. Physical Review B, 2009. **80**(8): p. 085202.
47. Kandemir, E.B., et al., *Modeling of the atomic structure and electronic properties of amorphous GaN<sub>1-x</sub>As<sub>x</sub>*. Computational Materials Science, 2014. **82**: p. 100-106.
48. Deng, H.X., et al., *Electronic origin of the conductivity imbalance between covalent and ionic amorphous semiconductors*. Physical Review B, 2013. **87**(12): p. 125203.
49. Pearce, C.I., R.A.D. Patrick, and D.J. Vaughan, *Electrical and magnetic properties of sulfides*. Sulfide Mineralogy and Geochemistry, 2006. **61**: p. 127-180.
50. Liu, J., A.X. Wei, and Y. Zhao, *Effect of different complexing agents on the properties of chemical-bath-deposited ZnS thin films*. Journal of Alloys and Compounds, 2014. **588**: p. 228-234.
51. Skinner, B.J., *Unit-Cell Edges of Natural and Synthetic Sphalerites*. American Mineralogist, 1961. **46**(11-2): p. 1399-1411.
52. Pham, H.H. and L.W. Wang, *Electronic structures and current conductivities of B, C, N and F defects in amorphous titanium dioxide*. Physical Chemistry Chemical Physics, 2015. **17**(17): p. 11908-11913.
53. Henkelman, G. and H. Jonsson, *Improved tangent estimate in the nudged elastic band method for finding minimum energy paths and saddle points*. Journal of Chemical Physics, 2000. **113**(22): p. 9978-9985.